

## Notes on the formation of interstellar H<sub>2</sub>

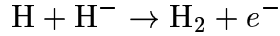
J. H. Black

*(History: 2000 January 15; revised 2001 March 26 and 2004 April 7)*

*Introduction.* Two major questions remain about the association of H atoms on grain surfaces to form H<sub>2</sub>: what is the effective rate of the process in the interstellar medium and what is the distribution of nascent molecules among excited vibration-rotation states. Recent experimental studies and theoretical treatments of H-atom association on astrophysically relevant surfaces represent important progress and help to clarify crucial issues. Pirronello et al. (1997a,b; 1999) presented measurements of molecular hydrogen formation on olivine and carbonaceous substrates at low temperatures (< 30 K). They concluded that adsorbed H atoms are not nearly as mobile as assumed by Hollenbach & Salpeter (1971) and that the effective formation rate in the interstellar medium may be approximately an order of magnitude lower than found in that classic study. Katz et al. (1999) modelled these laboratory measurements in a way that permits direct extension to interstellar conditions, while Biham et al. (1998) have already discussed the behavior of two limiting cases in **steady state**. There are several points that deserve further investigation. First, the steady state formulation may not be relevant for the interesting question of the evolution of an atomic cloud into a molecular cloud, because the time-dependence of the grain surface coverage and desorption processes are important. Second, when a grain surface is sparsely covered by H atoms, the effective formation rate **per grain** seems to have a quadratic dependence on the surface area (Biham et al. 1998), although other factors favoring the smallest grains may be buried in the coefficients of diffusion and desorption. Thus it will be important to determine whether the time dependence of the effective H<sub>2</sub> formation rate itself must be included in time-dependent chemical networks. In any case, the effective formation rate must be computed for a realistic distribution of grain sizes. It is of particular interest to understand whether the very small grains (sizes  $\lesssim 0.01 \mu\text{m}$ ) contribute to the formation of H<sub>2</sub>. If so, they may compensate partly for a reduced formation efficiency on classical dust grains compared with the model of Hollenbach & Salpeter (1971). If large molecules (e.g. polycyclic aromatic hydrocarbons = PAHs) act like very small grains, might they be important sites of H-atom association for form H<sub>2</sub>? Recent discussions of H-atom association on PAH cations offer conflicting results (Pauzat 2000; Herbst and Le Page 1999, Bauschlicher 1998). Finally, whenever interstellar grains reach low equilibrium temperatures in quiescent clouds, they are likely to accrete mantles of ices. Thus it is of interest to consider whether ice alters the efficiency of the H<sub>2</sub> formation process. Recent laboratory measurements of molecular hydrogen formation on amorphous water ice indicate that the formation efficiency remains high (Manicó et al. 2001).

It should also be noted that an unorthodox conjecture about the formation of interstellar H<sub>2</sub> has recently been published (Field 2000). Interstellar grains in the diffuse interstellar medium are expected to have an excess (negative) electrical charge of the order of one (or a few) electrons. If there is weak binding of electrons to the solid, then a hydrogen atom striking the surface may capture an electron and leave as a negative ion, H<sup>-</sup>. As pointed out by Field, this process can be a very large source of H<sup>-</sup> without violating

any known properties of materials that probably compose interstellar grains. With such a large source of  $\text{H}^-$ , the well known gas-phase process



can rival conventional grain-surface association as a source of interstellar  $\text{H}_2$ . This hypothesis is testable by astronomical observations, some of which are currently being carried out. One nice feature of this mechanism is that the distributions of kinetic energy and internal energy states for the newly formed molecules are predictable (Launay et al. 1991).

*A theory of the  $\text{H}_2$  formation rate*

Katz et al. (1999) have formulated a description of the  $\text{H}_2$  production rate that accurately represents the results of laboratory measurements of  $\text{H}_2$  association on analogues of interstellar grain surfaces at low temperatures. This description can be extended directly to the interstellar case, and Biham et al. (1998) have discussed some consequences of such a treatment. Further interesting implications are derived here.

The production rate of  $\text{H}_2$  per grain of diameter  $a$  is given by

$$R(a) = (1 - \mu)\alpha N_1^2 P_2 N_2 \quad \text{s}^{-1} \quad (1)$$

where  $N_1$  is the coverage (in monolayers) of H atoms on the surface and  $N_2$  is the coverage (in monolayers) of  $\text{H}_2$  molecules. These coverage functions are solutions of the rate equations

$$\frac{d}{dt}N_1 = F(1 - N_1 - N_2) - P_1 N_1 - 2\alpha N_1^2 \quad (2)$$

$$\frac{d}{dt}N_2 = \mu\alpha N_1^2 - P_2 N_2 \quad (3)$$

where

$$F = n(\text{H})v_{\text{H}}\sigma\xi(T_s) \quad \text{s}^{-1} \quad (4)$$

is the effective flux of H including a possible temperature-dependent sticking coefficient ( $\xi(T_s)$ ),

$$P_1 = \nu_0 \exp(-E_1/kT_s) \quad \text{s}^{-1} \quad (5)$$

is the desorption coefficient that describes the loss of H atoms from the surface of temperature  $T_s$ ,

$$P_2 = \nu_0 \exp(-E_2/kT_s) \quad \text{s}^{-1} \quad (6)$$

is the desorption coefficient that describes the loss of trapped  $\text{H}_2$  from the surface,

$$\alpha = \nu_0 \exp(-E_0/kT_s) \quad \text{s}^{-1} \quad (7)$$

is the hopping rate of H on the surface,  $\mu$  is the fraction of  $\text{H}_2$  molecules that remains on the surface following formation,  $(1 - \mu)$  is the fraction of  $\text{H}_2$  that is spontaneously desorbed,

$$\sigma = \pi a^2 \quad \text{cm}^2 \quad (8)$$

is the surface area of a spherical dust grain of diameter  $a$ , and

$$v_{\text{H}} = \left( \frac{8kT}{\pi m_{\text{H}}} \right)^{1/2} = 1.449 \times 10^4 T^{1/2} \text{ cm s}^{-1} \quad (9)$$

is the mean thermal speed of H at a gas temperature  $T$  where the number density is  $n(\text{H})$ . The fundamental frequency  $\nu_0$  (called the attempt rate by Katz et al.) is assumed to have the same value  $\nu_0 = 10^{12} \text{ s}^{-1}$  for desorption of H, desorption of  $\text{H}_2$ , and hopping, even though the activation barriers of these processes,  $E_1$ ,  $E_2$ , and  $E_0$ , respectively, have different sizes.

Equations (2) and (3) can be solved analytically in the limit of steady state. Note that these solutions as presented by Katz et al. (1999: their equations 10a,b) contain typographical errors. The corrected steady-state solutions are

$$N_1 \sim \frac{-(P_1 + F) + ((P_1 + F)^2 + 4\alpha F(2 + \mu F/P_2))^{1/2}}{2\alpha(2 + \mu F/P_2)} \quad (10)$$

and

$$N_2 \sim \mu\alpha N_1^2/P_2 \quad (11)$$

Biham et al. (1998) discussed the character of the steady state solutions and the limiting cases that apply in astronomical environments; however, they did not explore quantitatively how long it takes to reach steady state for conditions of interest.

The numerical solution of equations (2) and (3) is readily carried out through use of a standard differential equation solver, such as the Gear algorithm. Some preliminary results are summarized in the attached table. In these computations, a particle-size distribution

$$dn_g(a) = An_{\text{H}}a^\gamma da \quad (12)$$

has been adopted, with  $\gamma = -3.5$ . This is equivalent to the standard MRN particle-size distribution of Mathis, Rumpl, and Nordsieck (1977). This distribution is normalized with  $A = 1.861 \times 10^{-15}$  for  $a \in (0.005, 0.25) \mu\text{m}$ . This normalization corresponds to a dust/gas ratio of 0.01 by mass for a mean density of  $2.5 \text{ g cm}^{-3}$  in a silicate/graphite mixture. Then the integrated production rate of  $\text{H}_2$  is given by

$$\mathcal{R} = \int_{a_{\text{min}}}^{a_{\text{max}}} R(a)dn_g(a) = An_{\text{H}} \int_{a_{\text{min}}}^{a_{\text{max}}} a^{-3.5} R(a) da \quad (13)$$

and the effective binary rate coefficient, by

$$R_{\text{eff}} = \mathcal{R}/(n(\text{H})n_{\text{H}}) \text{ cm}^3 \text{ s}^{-1}. \quad (14)$$

This effective binary rate coefficient can be compared directly with the expression of Hollenbach et al. (1971)

$$R_{\text{HWS}}n(\text{H})n_{\text{H}} = \frac{1}{2}n(\text{H})v_{\text{H}}\sigma y_f n_g \quad (15)$$

where  $y_f$  is the combined efficiency of sticking and association (i.e. the fraction of H atoms striking the surface that forms a molecule in the gas). If we adopt

$$n_g\sigma = 3.1 \times 10^{-22} n_H \quad (16)$$

as implied by the average gas/extinction ratio in diffuse molecular clouds

$$N_H = 1.59 \times 10^{21} A_V \text{ cm}^{-2} \quad (17)$$

and the relation

$$A_V \approx Q_V \sigma N_g \approx 2\sigma N_g \quad (18)$$

then

$$R_{\text{HWS}} = 2.25 \times 10^{-18} T^{1/2} y_f \text{ cm}^3 \text{ s}^{-1} \quad (19)$$

The time-dependent formation rate is computed as outlined above by means of a numerical solution of the coupled equations (2) and (3). Then the effective binary rate coefficient  $R_{\text{eff}}$  is computed by an integration over the particle-size distribution. It is possible to evaluate a recombination efficiency

$$\eta = 2R(a)/F \quad (20)$$

at each value of the particle diameter  $a$ . This can be used as one measure of the relative importance of particles of different sizes.

### *Discussion of results*

The accompanying table summarizes results of the computations for two different grain materials, silicate and amorphous carbon. One motivation for performing the fully time-dependent calculation with a realistic particle-size distribution was to explore whether the formation rate coefficient itself must be computed as part of an evolutionary model of the chemistry of the interstellar medium. Note that for surface temperatures  $T_{\text{surf}} > 8$  K in silicates and  $T_{\text{surf}} > 13.5$  K in carbon, the time to reach steady state is always less than 1 year. Thus it appears that the steady state limits can be applied whenever the dust temperature is appropriate for the diffuse interstellar medium. At low temperatures in dark clouds, the time-scale for accretion of heavy atoms and molecules to form icy mantles is probably short enough that bare silicate or carbon surfaces are no longer relevant anyway. Since the recent experiments (Manicó et al. 2001) to measure H<sub>2</sub> formation on amorphous water suggest a high efficiency ( $y_f \sim 0.35$  in equations 15 and 19), it may be justifiable to apply the classical theory, equations 15–19, in the limit of cold dust. On the other hand, the new theory may need to be modified for application to photon-dominated regions (PDRs) of molecular clouds, where the lifetimes of molecules and dust particles against absorption of light can be quite short.

The laboratory experiments and the associated theoretical model have interesting implications for the formation rate in the diffuse interstellar medium and in PDRs. The formation efficiency can be very sensitive to the surface temperature of the dust. The

interpretation of COBE observations of the submm and far-IR background radiation of the Galaxy is complicated and there are conflicting conclusions in the literature: one model indicates that the radiating dust particles at high latitudes have temperatures between 13 and 17.5 K, for emissivity varying as  $\propto \nu^2$  (Legache et al. 1998), while other treatments derive dust temperatures in the range 18 to 22 K (Wright et al. 1991, Sodroski et al. 1997). Silicate particles with the adopted properties can form  $\text{H}_2$  with efficiencies  $y_f \approx 0.07$  to 0.4 at  $T_{\text{surf}} = 13$  K but are very inefficient at higher temperatures. In contrast, the amorphous carbon shows a broad peak in efficiency just in this temperature region, 13 – 17 K, with a corresponding mean efficiency  $y_f \sim 4$ . The implication may be that while silicate material does not form much  $\text{H}_2$  at  $T_{\text{surf}} \sim 15$  K, the carbonaceous component compensates with a very high formation efficiency.

Is it possible to make a simple, general conclusion about the rate of formation of  $\text{H}_2$  on grain surfaces when the formation rate depends on several parameters such as surface temperature, particle size, and material, as well as temperature and density of the gas? The above model of  $\text{H}_2$  formation can be used to make a completely self-consistent description of the atomic-to-molecular conversion in the interstellar medium. However, it also seems realistic to adopt the classical model of Hollenbach, Werner, and Salpeter (1971) with some mean value of the formation efficiency, e.g.  $y_f = 0.1$  to 0.3. The reason for this is that the detailed computations suggest that in a mixture of silicate and carbonaceous dust with a broad size distribution there will be some component of the dust that forms  $\text{H}_2$  with high efficiency over the entire reasonable range of surface temperatures.

*An alternative model: Cazaux & Tielens*

Cazaux and Tielens (2004) have noted that the model of Katz et al. (1999) considers physisorption of H only. Cazaux and Tielens argue that chemisorption will also be effective on interstellar dust surfaces. They show that inclusion of chemisorption and tunneling in the formation model permits  $\text{H}_2$  to continue forming with high efficiency even at high surface temperatures,  $T_{\text{dust}} \gtrsim 100$  K, while still reproducing the experimental results. Cazaux and Tielens (2002) used their alternative model to derive a simple expression for the association efficiency. In principle, that association efficiency could be incorporated into a calculation of an effective binary rate coefficient (equation 14) as described above.

Finally, we are developing in parallel a new code for modelling the abundance and excitation of  $\text{H}_2$  in interstellar clouds and PDRs. One of the first applications of this will be to extract better empirical constraints on the  $\text{H}_2$  formation rate from recent FUSE observations and from old Copernicus data.

*REFERENCES*

Bauschlicher, C.W., Jr. 1998, ApJ, 509, L125–L127; erratum, 1999, ApJ, 517, L67–L67  
 Biham, O., Furman, I., Katz, N., Pirronello, V., & Vidali, G. 1998, MNRAS, 296, 869–872  
 Cazaux, S., & Tielens, A. G. G. M. 2002, ApJ, 575, L29; erratum: 2002, ApJ, 577, L127  
 Cazaux, S., & Tielens, A. G. G. M. 2004, ApJ, 604, 222  
 Field, D. 2000, A&A, 362, 774–779  
 Herbst, E. & Le Page, V. 1999, A&A, 344, 310–316

Hollenbach, D.J. & Salpeter, E.E. 1971, ApJ, 163, 155–164.  
Hollenbach, D., Werner, M. W., & Salpeter, E. E. 1971, ApJ, 163, 155–164  
Katz, N., Furman, I., Biham, O., Pirronello, V., & Vidali, G. 1999, ApJ, 522, 305–312  
Lagache, G., Abergel, A., Boulanger, F., Puget, J.-L. 1998, A&A, 333, 709–720  
Launay, J. M., Le Dourneuf, M., & Zeippen, C. J.1991, A&A, 252, 842–852  
Manicó, G., Raguní, G., Pirronello, V., ROser, J. E., Vidali, G. 2001, ApJ, 548, L253–L256  
Mathis, J. S., Rumpl, W., Nordsieck, K. H.1977, ApJ, 217, 425–433  
Pauzat, F. 2000, *H<sub>2</sub> in Space*, editors F. Combes & G. Pineau des Forêts, (Cambridge: The University Press); electronic abstract only, article never published  
Pirronello, V., Biham, O., Liu, C., Shen, L., & Vidali, G. 1997a, ApJ, 483, L131–L134  
Pirronello, V., Liu, C., Shen, L., & Vidali, G. 1997b, ApJ, 475, L69–L72.  
Pirronello, V., Liu, C., Roser, J.E., & Vidali, G. 1999, A&A, 344, 681–686.  
Sodroski, T. J. et al. 1997, ApJ, 480, 173–187  
Wright, E. L. et al. 1991, ApJ, 381, 200–209

TABLE 1a. Computed H<sub>2</sub> formation rates: silicate (olivine)

Particle size spectrum (MRN):

normalizing constant A= 1.861E-15

Slope= -3.5,  $a_{\min} = 0.005$  and  $a_{\max} = 0.25 \mu\text{m}$

| $T_{\text{gas}}$ | $T_{\text{surface}}$ | $n(\text{H})$    | $R_{\text{eff}}$            | $t_{\text{ss}}$ | $\eta_{\text{max}}$ | $a(\eta_{\text{max}})$ |
|------------------|----------------------|------------------|-----------------------------|-----------------|---------------------|------------------------|
| K                | K                    | $\text{cm}^{-3}$ | $\text{cm}^3 \text{s}^{-1}$ | s               |                     | $\mu\text{m}$          |
| 10.              | 6.                   | 1.               | 1.20E-18                    | 1.33E+11        | 1.18E-01            | 5.0E-07                |
| 10.              | 7.                   | 1.               | 1.24E-17                    | 3.47E+10        | 7.63E-01            | 5.0E-07                |
| 10.              | 8.                   | 1.               | 3.23E-17                    | 2.94E+07        | 9.90E-01            | 5.0E-07                |
| 10.              | 9.                   | 1.               | 3.48E-17                    | 6.18E+05        | 9.88E-01            | 2.5E-06                |
| 10.              | 10.                  | 1.               | 3.01E-17                    | 2.08E+05        | 9.80E-01            | 2.0E-05                |
| 10.              | 11.                  | 1.               | 1.42E-17                    | 3.74E+04        | 9.30E-01            | 2.4E-05                |
| 10.              | 12.                  | 1.               | 3.61E-18                    | 1.49E+03        | 6.76E-01            | 2.4E-05                |
| 10.              | 13.                  | 1.               | 5.18E-19                    | 4.48E+02        | 2.12E-01            | 2.4E-05                |
| 100.             | 7.                   | 100.             | 4.00E-19                    | 8.04E+09        | 1.29E-02            | 5.0E-07                |
| 100.             | 8.                   | 100.             | 3.55E-17                    | 5.16E+06        | 7.20E-01            | 5.0E-07                |
| 100.             | 9.                   | 100.             | 9.14E-17                    | 1.01E+05        | 9.76E-01            | 5.0E-07                |
| 100.             | 10.                  | 100.             | 1.08E-16                    | 1.58E+04        | 9.80E-01            | 1.2E-06                |
| 100.             | 11.                  | 100.             | 1.03E-16                    | 3.55E+03        | 9.71E-01            | 6.0E-06                |
| 100.             | 12.                  | 100.             | 7.62E-17                    | 1.43E+03        | 9.60E-01            | 2.4E-05                |
| 100.             | 13.                  | 100.             | 3.65E-17                    | 4.20E+02        | 9.02E-01            | 2.4E-05                |
| 100.             | 14.                  | 100.             | 1.32E-17                    | 5.87E+01        | 7.11E-01            | 2.4E-05                |
| 100.             | 15.                  | 100.             | 3.68E-18                    | 4.97E+00        | 3.78E-01            | 2.4E-05                |
| 100.             | 16.                  | 100.             | 7.81E-19                    | 2.01E+00        | 1.14E-01            | 2.4E-05                |
| 100.             | 17.                  | 100.             | 1.58E-19                    | 2.69E-01        | 2.56E-02            | 2.4E-05                |
| 100.             | 6.                   | 1.               | 2.42E-20                    | 3.32E+12        | 7.84E-04            | 5.0E-07                |
| 100.             | 7.                   | 1.               | 2.21E-17                    | 2.14E+09        | 5.39E-01            | 5.0E-07                |
| 100.             | 8.                   | 1.               | 9.46E-17                    | 5.16E+06        | 9.83E-01            | 5.0E-07                |
| 100.             | 9.                   | 1.               | 1.10E-16                    | 4.14E+05        | 9.88E-01            | 1.5E-06                |
| 100.             | 10.                  | 1.               | 1.02E-16                    | 1.67E+05        | 9.80E-01            | 1.2E-05                |
| 100.             | 11.                  | 1.               | 6.10E-17                    | 1.59E+04        | 9.57E-01            | 2.4E-05                |
| 100.             | 12.                  | 1.               | 1.95E-17                    | 1.67E+03        | 8.00E-01            | 2.4E-05                |
| 100.             | 13.                  | 1.               | 3.94E-18                    | 4.48E+02        | 3.95E-01            | 2.4E-05                |
| 100.             | 14.                  | 1.               | 4.87E-19                    | 5.89E+01        | 7.45E-02            | 2.4E-05                |
| 100.             | 15.                  | 1.               | 5.84E-20                    | 9.99E+00        | 9.62E-03            | 2.4E-05                |
| 100.             | 17.                  | 1.               | 1.62E-21                    | 2.69E-01        | 2.69E-04            | 2.4E-05                |
| 1000.            | 8.                   | 1.               | 2.66E-16                    | 8.85E+06        | 9.68E-01            | 5.0E-07                |
| 1000.            | 9.                   | 1.               | 3.43E-16                    | 2.82E+05        | 9.88E-01            | 8.0E-07                |
| 1000.            | 10.                  | 1.               | 3.35E-16                    | 7.56E+04        | 9.80E-01            | 6.5E-06                |
| 1000.            | 11.                  | 1.               | 2.42E-16                    | 3.66E+04        | 9.69E-01            | 2.4E-05                |
| 1000.            | 12.                  | 1.               | 9.67E-17                    | 1.21E+03        | 8.80E-01            | 2.4E-05                |
| 1000.            | 13.                  | 1.               | 2.57E-17                    | 4.48E+02        | 5.85E-01            | 2.4E-05                |

|       |     |    |          |          |          |         |
|-------|-----|----|----------|----------|----------|---------|
| 1000. | 14. | 1. | 4.33E-18 | 5.89E+01 | 1.83E-01 | 2.4E-05 |
| 1000. | 15. | 1. | 5.74E-19 | 4.97E+00 | 2.92E-02 | 2.4E-05 |
| 1000. | 16. | 1. | 8.69E-20 | 5.29E-01 | 4.55E-03 | 2.4E-05 |
| 1000. | 17. | 1. | 1.62E-20 | 2.69E-01 | 8.50E-04 | 2.4E-05 |
| 1000. | 18. | 1. | 3.62E-21 | 1.59E-01 | 1.90E-04 | 2.4E-05 |

---



TABLE 1b. Computed H<sub>2</sub> formation rates: amorphous carbon

Particle size spectrum (MRN):

normalizing constant A= 1.861E-15

Slope= -3.5,  $a_{min} = 0.005$  and  $a_{max} = 0.25 \mu\text{m}$

| $T_{\text{gas}}$ | $T_{\text{surface}}$ | $n(\text{H})$    | $R_{\text{eff}}$             | $t_{\text{ss}}$ | $\eta_{\text{max}}$ | $a(\eta_{\text{max}})$ |
|------------------|----------------------|------------------|------------------------------|-----------------|---------------------|------------------------|
| K                | K                    | $\text{cm}^{-3}$ | $\text{cm}^3 \text{ s}^{-1}$ | s               |                     | $\mu\text{m}$          |
| 10.              | 10.                  | 1.               | 2.78E-21                     | 2.38E+13        | 2.85E-04            | 5.0E-07                |
| 10.              | 11.                  | 1.               | 3.55E-19                     | 4.92E+11        | 3.58E-02            | 5.0E-07                |
| 10.              | 12.                  | 1.               | 8.99E-18                     | 9.01E+09        | 6.26E-01            | 5.0E-07                |
| 10.              | 13.                  | 1.               | 2.45E-17                     | 7.34E+07        | 9.47E-01            | 5.0E-07                |
| 10.              | 14.                  | 1.               | 3.22E-17                     | 1.26E+07        | 9.87E-01            | 5.0E-07                |
| 10.              | 15.                  | 1.               | 3.46E-17                     | 3.74E+06        | 9.90E-01            | 8.0E-07                |
| 10.              | 16.                  | 1.               | 3.47E-17                     | 1.06E+06        | 9.86E-01            | 3.0E-06                |
| 10.              | 17.                  | 1.               | 3.28E-17                     | 9.20E+05        | 9.81E-01            | 1.0E-05                |
| 10.              | 18.                  | 1.               | 2.70E-17                     | 2.73E+05        | 9.76E-01            | 2.4E-05                |
| 10.              | 19.                  | 1.               | 1.73E-17                     | 3.86E+04        | 9.48E-01            | 2.4E-05                |
| 10.              | 20.                  | 1.               | 8.87E-18                     | 5.32E+04        | 8.67E-01            | 2.4E-05                |
| 10.              | 24.                  | 1.               | 1.12E-19                     | 3.29E+01        | 5.53E-02            | 2.4E-05                |
| 100.             | 12.                  | 100.             | 2.10E-19                     | 7.60E+09        | 6.79E-03            | 5.0E-07                |
| 100.             | 13.                  | 100.             | 5.61E-18                     | 9.87E+07        | 1.68E-01            | 5.0E-07                |
| 100.             | 14.                  | 100.             | 3.70E-17                     | 1.62E+06        | 7.22E-01            | 5.0E-07                |
| 100.             | 15.                  | 100.             | 7.33E-17                     | 3.83E+05        | 9.32E-01            | 5.0E-07                |
| 100.             | 16.                  | 100.             | 9.50E-17                     | 1.45E+05        | 9.76E-01            | 5.0E-07                |
| 100.             | 17.                  | 100.             | 1.05E-16                     | 1.42E+04        | 9.81E-01            | 6.0E-07                |
| 100.             | 18.                  | 100.             | 1.08E-16                     | 1.21E+04        | 9.76E-01            | 1.7E-06                |
| 100.             | 19.                  | 100.             | 1.05E-16                     | 4.00E+03        | 9.71E-01            | 4.5E-06                |
| 100.             | 20.                  | 100.             | 9.61E-17                     | 1.87E+03        | 9.65E-01            | 1.0E-05                |
| 100.             | 21.                  | 100.             | 7.80E-17                     | 1.01E+03        | 9.58E-01            | 2.4E-05                |
| 100.             | 22.                  | 100.             | 5.43E-17                     | 3.44E+02        | 9.40E-01            | 2.4E-05                |
| 100.             | 23.                  | 100.             | 3.36E-17                     | 3.99E+02        | 8.90E-01            | 2.4E-05                |
| 100.             | 24.                  | 100.             | 1.91E-17                     | 8.97E+01        | 7.94E-01            | 2.4E-05                |
| 100.             | 25.                  | 100.             | 1.01E-17                     | 4.29E+01        | 6.43E-01            | 2.4E-05                |
| 100.             | 26.                  | 100.             | 4.88E-18                     | 7.69E+00        | 4.49E-01            | 2.4E-05                |
| 100.             | 27.                  | 100.             | 2.12E-18                     | 6.26E+00        | 2.58E-01            | 2.4E-05                |
| 1000.            | 10.                  | 1.               | 2.79E-21                     | 4.81E+13        | 2.85E-05            | 5.0E-07                |
| 1000.            | 12.                  | 1.               | 1.81E-17                     | 9.71E+09        | 1.72E-01            | 5.0E-07                |
| 1000.            | 13.                  | 1.               | 1.43E-16                     | 4.06E+07        | 7.97E-01            | 5.0E-07                |
| 1000.            | 14.                  | 1.               | 2.65E-16                     | 3.33E+06        | 9.61E-01            | 5.0E-07                |
| 1000.            | 15.                  | 1.               | 3.25E-16                     | 9.87E+05        | 9.87E-01            | 5.0E-07                |
| 1000.            | 16.                  | 1.               | 3.44E-16                     | 4.06E+05        | 9.86E-01            | 1.0E-06                |
| 1000.            | 17.                  | 1.               | 3.43E-16                     | 9.82E+04        | 9.81E-01            | 3.5E-06                |
| 1000.            | 18.                  | 1.               | 3.23E-16                     | 3.10E+04        | 9.76E-01            | 9.0E-06                |

|       |     |    |          |          |          |         |
|-------|-----|----|----------|----------|----------|---------|
| 1000. | 19. | 1. | 2.68E-16 | 1.82E+04 | 9.71E-01 | 2.4E-05 |
| 1000. | 20. | 1. | 1.81E-16 | 6.68E+03 | 9.50E-01 | 2.4E-05 |
| 1000. | 21. | 1. | 1.02E-16 | 6.24E+03 | 8.87E-01 | 2.4E-05 |
| 1000. | 22. | 1. | 5.07E-17 | 1.36E+03 | 7.57E-01 | 2.4E-05 |
| 1000. | 23. | 1. | 2.22E-17 | 1.86E+02 | 5.46E-01 | 2.4E-05 |
| 1000. | 24. | 1. | 8.31E-18 | 5.48E+01 | 3.02E-01 | 2.4E-05 |

---